MRS Communications (2018), *8*, 1321–1327

doi:10.1557/mrc.2018.159

MRS Communications

Research Letter

Strategies for elemental mapping from energy-filtered TEM of polymeric materials

Brooke Kuei, Department of Materials Science and Engineering, The Pennsylvania State University, University Park, PA 16802, USA
Bernd Kabius, and **Jennifer L. Gray,** Materials Research Institute, The Pennsylvania State University, University Park, PA 16802, USA
Enrique D. Gomez, Department of Materials Science and Engineering, The Pennsylvania State University, University Park, PA 16802, USA; Materials Research Institute, The Pennsylvania State University, University Park, PA 16802, USA; Department of Chemical Engineering, The Pennsylvania State University, University Park, PA 16802, USA

Address all correspondence to Enrique D. Gomez at **edg12@psu.edu**

(Received 22 June 2018; accepted 27 July 2018)

Abstract

Energy-filtered transmission electron microscopy provides an opportunity to map the nanoscale elemental composition in polymeric systems. Nevertheless, it presents its own set of unique challenges in its application to soft materials. Here, we outline an optimized protocol for elemental mapping in soft materials using sulfur mapping of polymer/fullerene mixtures as an example. Three factors are crucial: (1) focusing at zero-loss, (2) using an objective aperture, and (3) maximizing signal-to-noise and counts for the chosen imaging conditions. Analyzing the corresponding source images, bright field images, and thickness maps can ensure optimum conditions are achieved for elemental mapping of polymers.

Introduction

Transmission electron microscopy (TEM) has contributed to many advances in polymer and soft matter science. Some of the earliest applications of TEM for polymers revealed spherulitic crystallization of natural rubber and low-density polyethylene.[1] Later, TEM studies of lamellar crystals of polyethylene led to the folded chain model.[2] These pioneering studies relied on standard bright-field techniques with the aid of gold or chromium shadowing to generate contrast in the TEM, but as the need arose to image more complex systems, such as blends and block copolymers, new modalities for imaging became warranted.

Most TEM studies of polymeric materials rely on mass contrast, where the image intensity depends on local mass thickness (thickness multiplied by density). Nevertheless, polymeric materials are generally composed of elements with low atomic numbers where domains have little or no difference in electron density. One strategy has been to use heavy element stains, but staining can perturb the morphology and specificity relies on differences in physical absorption or chemical reactivity, which depend on the details of the system.

Alternatively, the image formation process can rely on phase and diffraction contrast.[3] Phase contrast relies on defocus of the objective lens to provide interference between the scattered and unscattered beam based on differences in the mean inner potential, but the contrast enhancement is often modest and resolution is limited due to defocus. If one of the materials is crystalline, dark field imaging using an objective aperture to select a scattered beam can distinguish between different phases through diffraction contrast. Given the sensitivity of polymers to radiation damage, this approach is often limited to electron doses of about 20 e/Å^2,[4] limiting the capture of multiple orientations or reflections, resulting in an incomplete picture of the distribution of crystallites in any single image. As a consequence, moving beyond mass, phase, and diffraction contrast will be transformative, especially for studies of more complex structures.

Analytical TEM aims to supplement the aforementioned contrast mechanisms, such as through energy-filtered TEM (EFTEM), which relies on inelastically scattered electrons for the image formation process. As the electron beam interacts with the sample, inelastic losses will be a consequence of the valence electronic structure (1–10 eV), from plasmon resonances (10–50 eV), or from excitations of core-shell electrons (50–1000 eV). These electrons can be discriminated by their energy-loss by magnetic fields applied in spectrometers because they will be deflected to different angles depending on their energies. An energy filter can then be used to form images at a user-defined energy-loss, which is selected by a slit aperture in the energy-dispersive plane of the spectrometer. Currently, there are two types of energy filters available, in-column Ω-filters and post-column energy filters called Gatan imaging filters (GIFs). These energy filters can then provide imaging modalities beyond mass, phase, and diffraction contrast.

While conventional bright-field imaging of polymeric materials suffers from minimal mass contrast, polymer systems have

been successfully imaged using EFTEM to generate contrast from differences in the valence electronic structure,[5] elemental composition,[6–9] or plasmons absorption.[10–14] Nevertheless, the weak mass contrast inherent to many soft materials systems provides unique challenges. Here, we outline an optimized protocol for elemental mapping in soft materials using sulfur mapping of the polymer/fullerene blend poly(3-hexylthiophene-2,5-diyl)/[6,6]-phenyl-C61-butyric acid methyl ester (P3HT/PCBM) as an example. We emphasize that three factors are crucial: (1) focusing at zero-loss, (2) using an objective aperture, and (3) maximizing signal-to-noise and counts.

Materials and methods

15 mg/mL solutions of P3HT (50.9 kg/mol, Đ of 2.23, 96% H-T regioregularity, Merck) and PCBM (Merck) (in 1:1 ratio) were made with chlorobenzene (Sigma-Aldrich) in a nitrogen glove box and stirred for a minimum of 10 h at 45 °C. Silicon wafers were cleaned through sonication for 20 min in acetone and 20 min in isopropanol followed by 15 min of ultraviolet light ozonation. PEDOT:PSS (Clevios P, H.C. Starck) was spin-cast onto the silicon wafers in air, after which P3HT/PCBM was spin-cast onto the PEDOT:PSS film inside a nitrogen glove box. Films (ca. 70 ± 10 nm) were floated off in deionized water and then picked up with copper TEM grids. Samples were dried overnight at room temperature under vacuum and then annealed at 190 °C for 45 min in a nitrogen glove box. Sulfur elemental maps were taken at the Penn State Materials Characterization Lab on the Tecnai G2 20 XTWIN operating at 200 kV equipped with a GIF Tridiem filter and the FEI Titan Krios operating at 300 kV equipped with a GIF Quantum filter and K2 direct electron detector using the standard three-window method.[15] A slit width of 20 eV was used. Pre-edge 1, pre-edge 2, and post-edge energies were 128, 150, and 185 eV, respectively. The size of the objective aperture used was 20 μm.

Results and discussion

Generating elemental maps from core-loss energy filtered micrographs

As the electron beam interacts with the sample, electrons will scatter elastically and inelastically. A magnetic prism beneath the TEM can separate scattered electrons into their respective energy losses, after which a slit is used to select only electrons of a specified energy loss to create the image. Selecting only elastically scattered electrons, for example, will generate a zero-loss image, which has improved contrast compared with an unfiltered image due to the larger inelastic scattering cross-section (when compared with elastic cross-sections) of organic materials.[15,16] As shown for P3HT/PCBM mixtures, the zero-loss [Fig. 1(b)] and unfiltered images [Fig. 1(a)] can be used to calculate a thickness map [Fig. 1(c)].

Often there is little mass contrast in zero-loss images for polymeric materials because differences in density are small. As a consequence, many TEM micrographs of polymers rely on chemical or physical selective staining with heavy elements to generate imaging contrast.[17] Instead, we can use core-loss electrons to obtain elemental maps. This is most commonly accomplished using the three-window method, in which two pre-edge images [Figs 1(d) and 1(e)] and one post-edge image [Fig. 1(f)] is acquired. The energy window selected for the three energy-filtered micrographs are optimized from the electron energy-loss spectrum near the edge of interest; for P3HT/PCBM this was 128, 150, and 185 eV with a ±10 eV window (20 eV slit). The two pre-edge images are used to generate a background that is then subtracted from the post-edge image, resulting in an elemental map [Fig. 1(g)]. The thickness t of the sample should be much thinner than the mean free path λ to ensure low plural scattering and mass thickness contributions to the image;[15] in Fig. 1(g) t/λ is on average 0.2.

The comparison between the thickness and elemental maps serve as confirmation that contrast in the elemental map is from elemental contrast and not thickness variations. The elemental map is directly proportional to the amount of sulfur, such that thicker regions are expected to show stronger sulfur signal even if the composition within the film is homogeneous and spatially invariant. Thus, differences between the sulfur map and thickness map indicate enrichment of sulfur composition within the film. Furthermore, a map of the sulfur composition (averaged over the thickness of the film) can be extracted by dividing the elemental map by the thickness map, as previously outlined.[18]

Previous work has demonstrated similar core-loss elemental maps as the one shown in Fig. 1 for P3HT/PCBM mixtures,[5,7,8,19–22] as well as for other conjugated polymer mixtures.[6,18,23–26] The goal of the following sections is to systematically outline the crucial parameters and common pitfalls that are needed to successfully generate elemental maps of polymeric systems. As we describe below, we propose that a complete set of images include a bright field micrograph, a thickness map, and an elemental map of the same region to minimize the possibility of artifacts affecting imaging results.

Focusing at zero-loss

Focusing at zero-loss is difficult because the lack of contrast in polymeric materials often causes the zero-loss image to look the same even at different defocus values. Ideally, we would be able to find focus at the sulfur edge, but in the case of electron-transparent polymer films, the counts at the sulfur edge are too low to practically tune the defocus. Furthermore, in some cases, elemental enrichment is anti-correlated with mass density, such that contrast at an elemental edge may be minimal or diminished. A common practice for EFTEM is to use the plasmon energy-loss to find focus, but contrast can also be weak in the plasmon region due to the broad, overlapping plasmon resonances between organic materials. To overcome these challenges, we have found that the use of Fast Fourier Transforms (FFTs) of the zero-loss image can guide the operator in finding focus. FFTs are routinely used to minimize astigmatism, and we propose that FFTs can also be used to minimize defocus when imaging low-contrast soft materials.

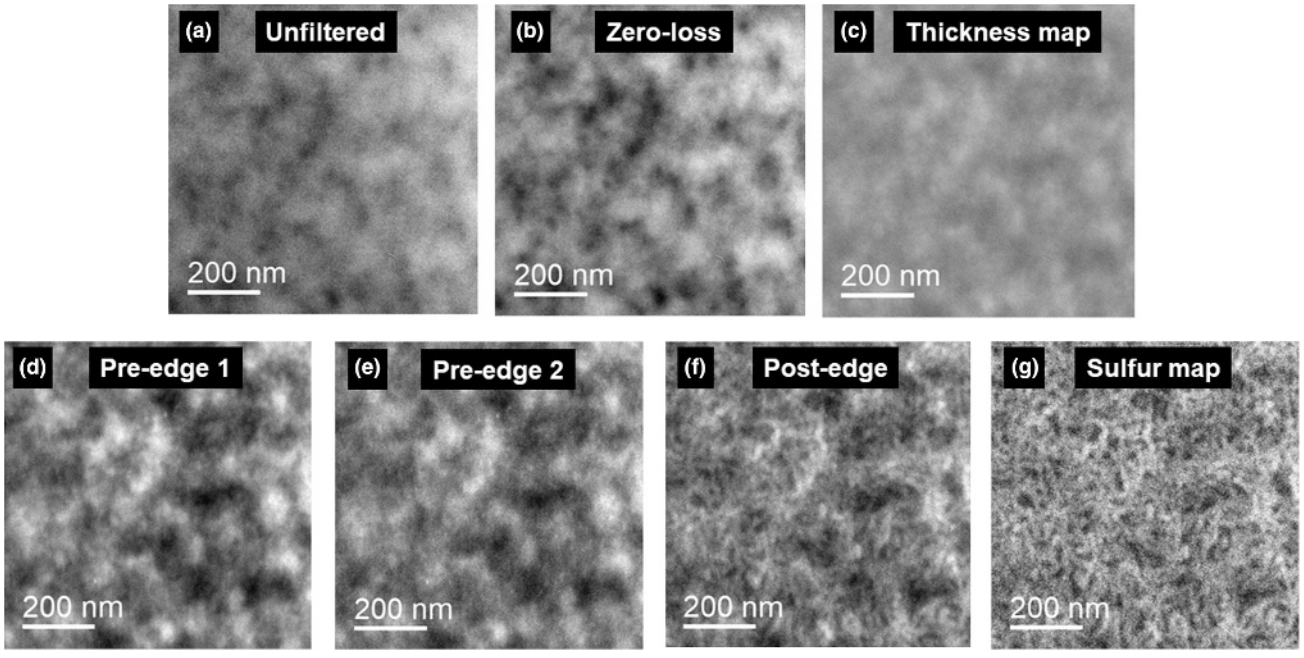

Figure 1. TEM images of P3HT/PCBM films. The unfiltered image (a) consists of both elastically and inelastically scattered electrons. The zero-loss image (b) is composed of only elastically scattered electrons. From the unfiltered and zero-loss image, a thickness map (c) can be generated. While zero-loss images of polymeric materials do not reveal much structure, elemental maps such as a sulfur map (g) can be generated through the three-window method, which uses two pre-edge images (d, e) to estimate a background that is subtracted from a post-edge image (f).

As shown in Fig. 2, zero-loss images of P3HT/PCBM mixtures show little contrast, where features mostly correspond to large-scale film thickness fluctuations. Thus, focusing by eye is challenging. Corresponding elemental maps show significant loss of resolution when the zero-loss image is out of focus; in this case, about 2–3 microns out of focus will cause a loss of resolution in 10 nm features (Fig. 2). The overall challenge of focusing for smaller features that are apparent in the bright field images (that require smaller defocus) can be resolved by relying on the FFTs to guide the operator to minimal defocus. The addition of sulfur-containing nanoparticles that do not disrupt morphology could also be a solution for perfecting focus of soft materials when taking sulfur elemental maps.

Using an objective aperture

We demonstrate that the use of an objective aperture improves contrast in elemental maps of polymeric materials (Fig. 3). The role of the objective aperture is to filter out electrons that have been scattered to high angles. Incoherent scattering, such as from multiple scattering, is angle-independent and will add a background or noise to images. From Bethe theory, the differential cross section for inelastic scattering decreases quickly at high scattering angles.[15] We hypothesize that the objective aperture is important because it removes electrons scattered to high angles that are mostly due to incoherent scattering; when the image formation process relies on inelastically scattered electrons the fraction of incoherently scattered electrons is likely higher. Although an alternative hypothesis is that the objective aperture is adding elastic contrast (mass contrast) to the image, thickness maps [Fig. 1(c)] do not show the same contrast as the sulfur maps shown in Fig. 1(g) or Fig. 3.

Maximizing signal-to-noise and counts

In order to generate high-quality sulfur maps, it is important to maximize signal-to-noise and to ensure that counts are above the noise level of the detector. Counts can be maximized by centering the beam on the charge-coupled device (CCD) and spreading the beam so that its circumference just barely surpasses the CCD screen; care must be taken that the curvature of the beam does not introduce defocus at the image edges. Qualitatively, sulfur maps taken with increasing exposure times (and therefore higher counts) show improved resolution (Fig. 4). Line scans of post-edge images show that signal-to-noise increases with increasing exposure time (Supplementary Fig. S1). Figure 4 and Supplementary Fig. S1 suggest that for a GIF Tridiem detector (UltraScan sensor with 2048 × 2048 pixels), about at least 200 counts is needed for all energy-filtered images to generate high-quality sulfur maps. We note that high doses are detrimental for soft materials; however, for heavy elements like sulfur, which are unlikely to diffuse, high doses are tolerated, such that we are effectively imaging sulfur atoms in a carbon-rich matrix due to damage.

To investigate the correlation between signal-to-noise and exposure time in more detail, we calculate a peak-to-noise

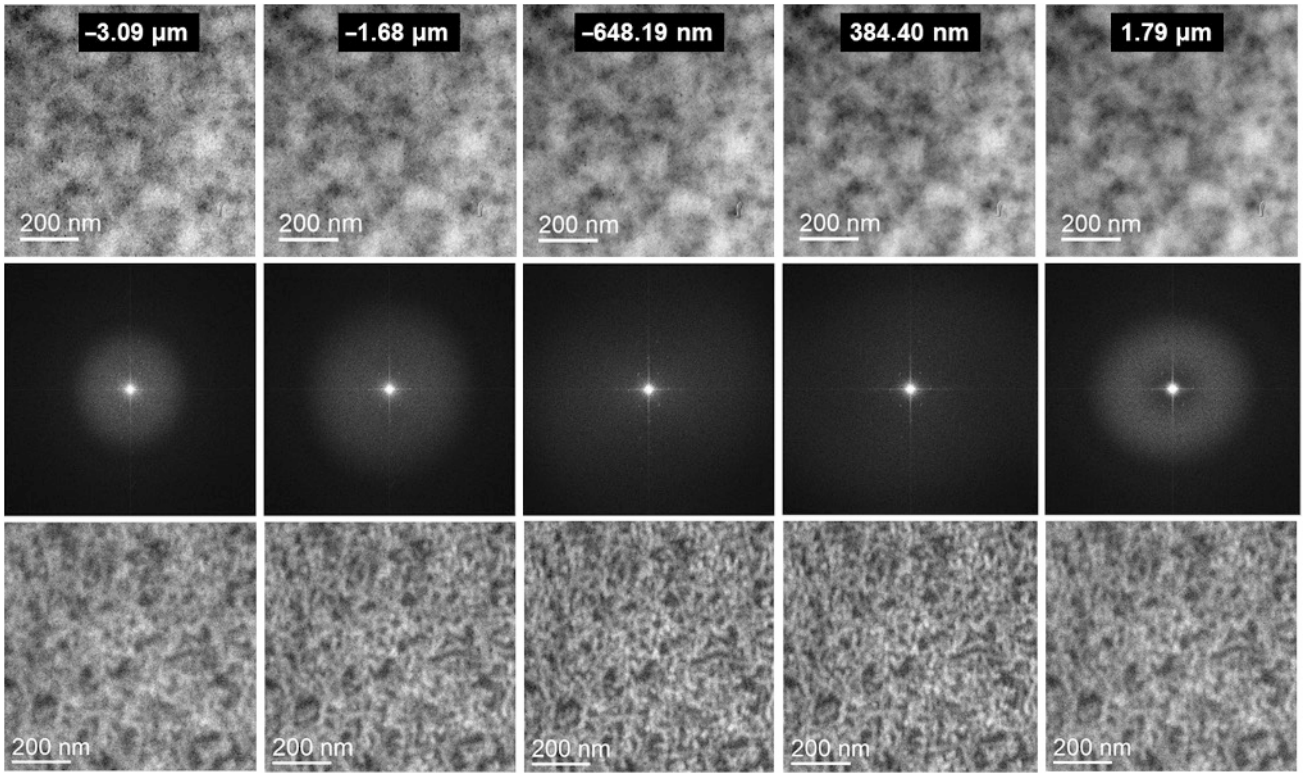

Figure 2. Zero-loss images (top row), corresponding FFTs (middle row), and resultant sulfur elemental maps (bottom row) at various defocus values. While all zero-loss images look similar, a few hundred nanometers of defocus can have a significant effect on resultant elemental maps.

ratio, which we define as the peak amplitude of a given feature in a line scan divided by the variance in intensity with respect to a moving average. This is exemplified in Supplementary Fig. S2 for one fiber feature; peak-to-noise ratios reported in Fig. 4 are averaged from three individual features. Peak-to-noise ratios approximately increase with the square root of exposure time.

Binning combines charges collected by adjacent CCD pixels; therefore, increased binning leads to an increase in signal-to-noise at the cost of resolution. We demonstrate elemental mapping of P3HT/PCBM using a range of binning at the same exposure time of 40 s (Supplementary Fig. S3), where the signal-to-noise increases with binning (Supplementary Fig. S4). The pixel size, however, increases from 0.41 nm for binning 1 to 3.31 nm

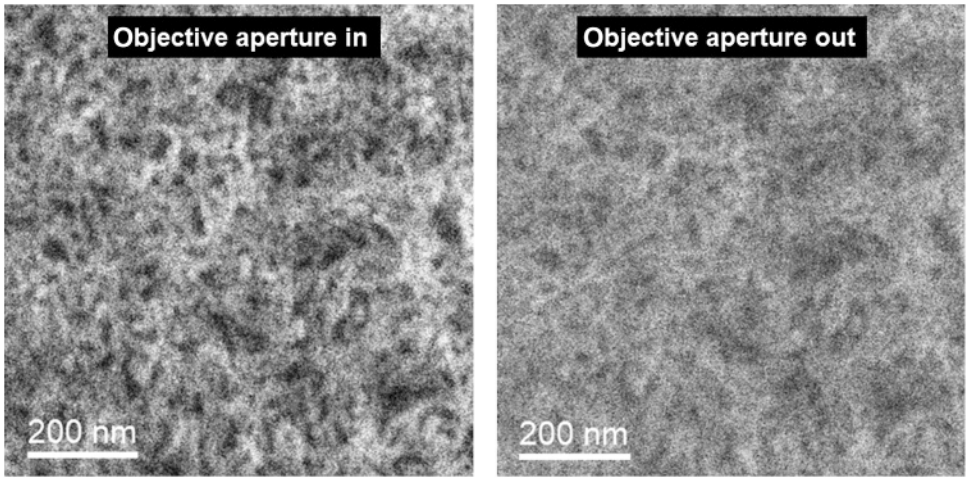

Figure 3. Sulfur elemental maps of P3HT/PCBM films acquired with an objective aperture (left) and without an objective aperture (right).

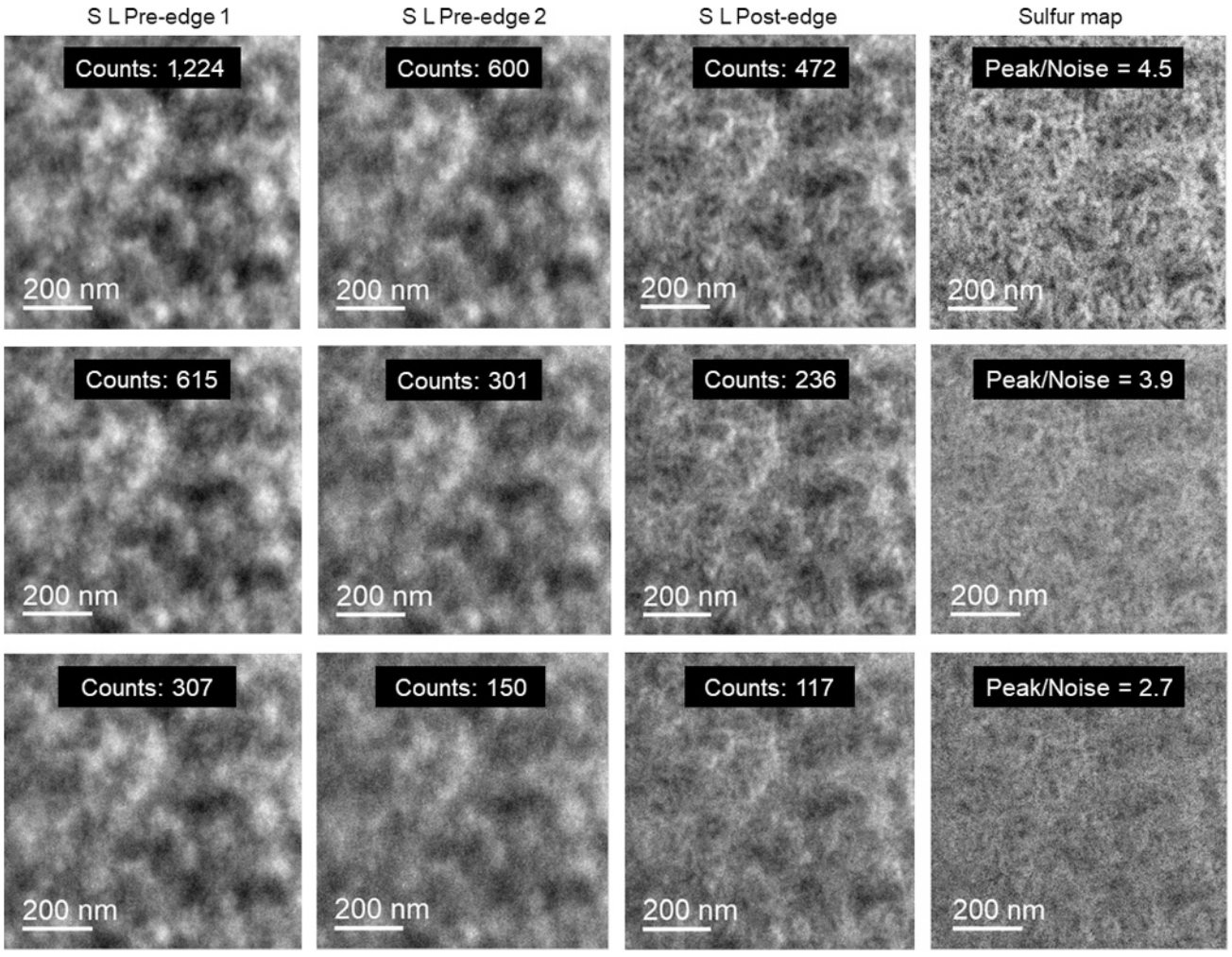

Figure 4. Source images and sulfur maps taken with a 40 s exposure (top), 20 s exposure (middle), and 10 s exposure (bottom). CCD counts are included for each source image and average peak-to-noise ratios are reported for each sulfur elemental map.

for binning 8 at a magnification of 33,800x. The peak-to-noise ratio at first increases linearly with increased binning but appears to saturate after binning 4, suggesting binning 4 is optimum for this feature size of interest (ca. 10 nm) at this magnification. Thus, careful optimization of both exposure time and binning are necessary to optimize imaging conditions. Furthermore, for samples with severe drift, a lower exposure time combined with higher binning is often ideal, as long as the trade-off with loss of resolution is acceptable for the feature size of interest. Although in principle counts can be increased to achieve the needed counts for high-quality elemental maps generated from core-loss energy-filtered images, in practice drift can limit the exposure time. A possibility to overcome this limitation is to use a series of short images that are drift corrected to achieve the needed counts, as is commonly done in single-particle reconstructions.[27]

Another strategy for increasing signal-to-noise is the use of a direct electron detector.[28] While a traditional CCD converts primary electrons into photons via a scintillator, a direct electron detector bypasses the scintillation step, thus leading to higher signal-to-noise. As shown in Supplementary Fig. S5, the peak-to-noise ratio of P3HT/PCBM sulfur elemental maps is approximately 1.5 higher for the K2 direct electron detector compared with a traditional UltraScan for the same sample at identical imaging conditions. Although these images are similar to elemental maps shown in Figs. 1–4, the microstructure differs slightly because a different P3HT batch was used. Nevertheless, Supplementary Fig. S5 demonstrates that for the same sample at identical imaging conditions, use of a direct electron detector can improve the signal-to-noise of a sulfur elemental map for polymeric materials.

Although this work is focused on sulfur elemental mapping, the outlined strategies are applicable for mapping at other edges, such as carbon, nitrogen, oxygen, and fluorine. It is often informative to map at two edges when possible, to further confirm the role of thickness variations in elemental maps. For

example, demonstrating a contrast inversion when mapping two different elements eliminates the possibility that both maps are representative of thickness variations.[7] We also expect that our approach outlined here can aid in mapping at the plasmon region (5 to 30 eV). Background subtraction and accounting for thickness variations require more images than the three-window method due to broad overlapping plasmon peaks for most materials, such that approaches like principal component analysis are needed.[5,12,29–31] Focusing on the plasmon region is easier simply because of the higher signal (when compared with core-loss imaging) that allows focusing directly at the energy loss of interest. Nevertheless, optimization of the imaging conditions is also crucial for plasmon imaging to aid in the identification of the contributions to the resulting plasmon maps.

Summary and conclusions

Polymer microscopy brings about a set of challenges that often differ from hard materials microscopy, such as low imaging contrast due to similar electron densities between amorphous or weakly diffracting phases or domains. Core-loss elemental mapping addresses this limitation by revealing the morphology through differences in elemental composition. Three factors are emphasized for successful elemental mapping of polymeric materials, including focusing at zero-loss, using an objective aperture, and ensuring sufficient signal-to-noise and counts, such as by binning pixels. We also propose that in order to minimize the probability of artifacts, FFTs of bright field images can ensure near zero defocus, thickness maps can confirm the thickness of the sample is less than the inelastic mean free path (and reveal regions where elemental maps could be dominated by mass contrast), and the counts of the source images can ensure enough signal reached the detector to allow for successful elemental mapping. Although in principle this technique could be limited by radiation damage, in the example highlighted here, mapping sulfur densities is tolerant to high radiation doses at the mesoscale, because damage results in sulfur within a carbon-rich matrix that diffuses slowly.

Supplementary material

The supplementary material for this article can be found at https://doi.org/10.1557/mrc.2018.159.

Acknowledgments

Funding for this work was provided by NSF DMR-1609417. BK also acknowledges support from the DOE Office of Science Graduate Student Research (SCGSR) Award, and the ALS Doctoral Fellowship in Residence. BK acknowledges Alex Grede for helpful discussions on noise analysis.

References

1. R. Eppe, E.W. Fischer, and H.A. Stuart: Morphologische strukturen in Polyathylenen, Polyamiden. *J. Polym. Sci.* **XXXIV**, 721 (1959).
2. D.C. Bassett, F.C. Frank, and A. Keller: Some new habit features in crystals of long chain compounds part IV. the fold surface geometry of monolayer polyethylene crystals and its relevance to fold packing and crystal growth. *Philos. Mag.* **8**, 1753 (1963).
3. C. Barry Carter and D.B. Williams: *Transmission Electron Microscopy* (Springer, New York, NY, 2009).
4. Z.J.W.A. Leijten, A.D.A. Keizer, G. de With, and H. Friedrich: Quantitative analysis of electron beam damage in organic thin films. *J. Phys. Chem. B.* **121**, 10552 (2017).
5. C. Guo, F.I. Allen, Y. Lee, T.P. Le, C. Song, J. Ciston, A.M. Minor, and E.D. Gomez: Probing local electronic transitions in organic semiconductors through energy-loss spectrum imaging in the transmission electron microscope. *Adv. Funct. Mater.* **25**, 6071 (2015).
6. D.R. Kozub, K. Vakhshouri, S.V. Kesava, C. Wang, A. Hexemer, and E.D. Gomez: Direct measurements of exciton diffusion length limitations on organic solar cell performance. *Chem. Commun.* **48**, 5859 (2012).
7. D.R. Kozub, K. Vakhshouri, L.M. Orme, C. Wang, A. Hexemer, and E.D. Gomez: Polymer crystallization of partially miscible polythiophene/fullerene mixtures controls morphology. *Macromolecules* **44**, 5722 (2011).
8. G.K. Mor, T.P. Le, K. Vakhshouri, D.R. Kozub, and E.D. Gomez: Elemental mapping of interfacial layers at the cathode of organic solar cells. *ACS Appl. Mater. Interfaces* **6**, 19638 (2014).
9. E.D. Gomez, A. Panday, E.H. Feng, V. Chen, G.M. Stone, A.M. Minor, C. Kisielowski, K.H. Downing, O. Borodin, G.D. Smith, and N. P. Balsara: Effect of ion distribution on conductivity of block copolymer electrolytes. *Nano Lett.* **9**, 1212 (2009).
10. L.F. Drummy, R.J. Davis, D.L. Moore, M. Durstock, R.A. Vaia, and J.W. P. Hsu: Molecular-scale and nanoscale morphology of P3HT:PCBM bulk heterojunctions: energy-filtered TEM and low-dose HREM†. *Chem. Mater.* **23**, 907 (2011).
11. A.A. Herzing, L.J. Richter, and I.M. Anderson: 3D Nanoscale characterization of thin-film organic photovoltaic device structures via spectroscopic contrast in the TEM. *J. Phys. Chem. C.* **114**, 17501 (2010).
12. F.I. Allen, M. Watanabe, Z. Lee, N.P. Balsara, and A.M. Minor: Chemical mapping of a block copolymer electrolyte by low-loss EFTEM spectrum-imaging and principal component analysis. *Ultramicroscopy* **111**, 239 (2011).
13. F.I. Allen, L.R. Comolli, A. Kusoglu, M.A. Modestino, A.M. Minor, and A.Z. Weber: Morphology of hydrated as-cast nafion revealed through cryo electron tomography. *ACS Macro Lett.* **4**, 1 (2014).
14. E.M. Linares, C.A.P. Leite, L.F. Valadares, C.A. Silva, C.A. Rezende, and F. Galembeck: Molecular mapping by low-energy-loss energy-filtered transmission electron microscopy imaging. *Anal. Chem.* **81**, 2317 (2009).
15. R.F. Egerton: *Electron Energy-Loss Spectroscopy in the Electron Microscope*, 3rd ed. (Springer, New York, 2011).
16. E.D. Gomez, M.L. Ruegg, A.M. Minor, C. Kisielowski, K.H. Downing, R.M. Glaeser, and N.P. Balsara: Interfacial concentration profiles of rubbery polyolefin lamellae determined by quantitative electron microscopy. *Macromolecules* **41**, 156 (2008).
17. L.C. Sawyer, D.T. Grubb, and G.F. Meyers: *Polymer Microscopy*, 3rd ed. (Springer, New York, 2008), pp. 146–160.
18. S.V. Kesava, Z. Fei, A.D. Rimshaw, C. Wang, A. Hexemer, J.B. Asbury, M. Heeney, and E.D. Gomez: Domain compositions and fullerene aggregation govern charge photogeneration in polymer/fullerene solar cells. *Adv. Energy Mat.* **4**, 1400116 (2014).
19. K. Vakhshouri, S.V. Kesava, D.R. Kozub, and E.D. Gomez: Characterization of the mesoscopic structure in the photoactive layer of organic solar cells: A focused review. *Mater. Lett.* **90**, 97 (2013).
20. S. Vajjala Kesava, R. Dhanker, D.R. Kozub, K. Vakhshouri, U.H. Choi, R.H. Colby, C. Wang, A. Hexemer, N.C. Giebink, and E.D. Gomez: Mesoscopic structural length scales in P3HT/PCBM mixtures remain invariant for various processing conditions. *Chem. Mater.* **25**, 2812 (2013).
21. K. Vakhshouri, D.R. Kozub, C. Wang, A. Salleo, and E.D. Gomez: Effect of miscibility and percolation on electron transport in amorphous poly (3-Hexylthiophene)/Phenyl-C61-Butyric Acid methyl ester blends. *Phys. Rev. Lett.* **108**, 026601 (2012).
22. C. Guo, D.R. Kozub, S.V. Kesava, C. Wang, A. Hexemer, and E.D. Gomez: Signatures of multiphase formation in the active layer of organic solar cells from resonant soft x-ray scattering. *ACS Macro Lett.* **2**, 185 (2013).

23. B. Kuei and E.D. Gomez: Chain conformations and phase behavior of conjugated polymers. *Soft Matter* **13**, 49 (2017).
24. M.A. Kelly, S. Roland, Q.Q. Zhang, Y.M. Lee, B. Kabius, Q. Wang, E.D. Gomez, D. Neher, and W. You: Incorporating fluorine substitution into conjugated polymers for solar cells: three different means, same results. *J. Phys. Chem. C.* **121**, 2059 (2017).
25. C. Lee, Y. Li, W. Lee, Y. Lee, J. Choi, T. Kim, C. Wang, E.D. Gomez, H.Y. Woo, and B.J. Kim: Correlation between phase-separated domain sizes of active layer and photovoltaic performances in all-polymer solar cells. *Macromolecules* **49**, 5051 (2016).
26. Z.H. Mao, W. Senevirathna, J.Y. Liao, J. Gu, S.V. Kesava, C.H. Guo, E.D. Gomez, and G. Sauve: Azadipyrromethene-based Zn(II) complexes as nonplanar conjugated electron acceptors for organic photovoltaics. *Adv. Mater.* **26**, 6290 (2014).
27. A. Doerr: Single-particle cryo-electron microscopy. *Nat. Methods* **13**, 23 (2015).
28. J.L. Hart, A.C. Lang, A.C. Leff, P. Longo, C. Trevor, R.D. Twesten, and M. L. Taheri: Direct detection electron energy-loss spectroscopy: a method to push the limits of resolution and sensitivity. *Sci. Rep.* **7**, 8243 (2017).
29. S. Yakovlev, and M. Libera: Dose-limited spectroscopic imaging of soft materials by low-loss EELS in the scanning transmission electron microscope. *Micron* **39**, 734 (2008).
30. L.F. Drummy, R.J. Davis, D.L. Moore, M. Durstock, R.A. Vaia, and J.W. P. Hsu: Molecular-scale and nanoscale morphology of P3HT:PCBM bulk heterojunctions: energy-filtered TEM and low-dose HREM. *Chem. Mater.* **23**, 907 (2011).
31. L.A. Perez, J.T. Rogers, M.A. Brady, Y. Sun, G.C. Welch, K. Schmidt, M.F. Toney, H. Jinnai, A.J. Heeger, M.L. Chabinyc, G.C. Bazan, and E.J. Kramer: The role of solvent additive processing in high performance small molecule solar cells. *Chem. Mater.* **26**, 6531 (2014).